available at www.sciencedirect.com

ScienceDirect

journal homepage: www.elsevier.com/locate/compag

Shape identification and particles size distribution from basic shape parameters using ImageJ

C. Igathinathane, L.O. Pordesimo, E.P. Columbus, W.D. Batchelor, S.R. Methuku*

Agricultural and Biological Engineering Department, Mississippi State University, 130 Creelman Street, Mississippi State, MS 39762, USA

ARTICLE INFO

Article history:
Received 29 August 2007
Received in revised form
13 December 2007
Accepted 24 February 2008

Keywords:
ImageJ
Image processing
Machine vision
Physical properties
Plugin
Shape identification

ABSTRACT

Quick and accurate particle size distribution analysis is desirable in various technical fields that handle granular or particulate materials including size reduction. We developed an ImageJ plugin that extracts the dimensions from a digital image of disjoint particles after identifying their shapes and determines their particles size distribution. We established that the major and minor axes of ImageJ fitted ellipse along with the developed correction factors efficiently determined dimensions of particles. This paper describes the plugin development and its application to food grains and ground biomass. Using computer generated geometrical shapes as reference objects, a shape identification strategy that addresses common geometric shapes such as square, inclined square, rectangle, inclined rectangle, circle, ellipse, and inclined ellipse was developed. The strategy used only three newly defined shape parameters to identify objects, such as reciprocal aspect ratio, rectangularity, and feret major axis ratio from the standard outputs generated by ImageJ. Evaluation of effects of the particles shape, size, and orientation on the deviation from the reference particle's length and width indicated that the mean absolute deviations of all these factors were less than 1.3%. Developed plugin was applied successfully to analyze the dimensions and size distribution of food grains and ground Miscanthus particles images. The plugin produced quick and accurate size distribution of particles from digital images and can be applied to variety of particle analysis applications.

1. Introduction

Computer vision-based image processing methods have been investigated as an alternative to provide solutions to practical measurement, identification, and size distribution analysis. Achieving similar outputs with manual means will be time consuming and painstaking; therefore, several reported research works explored the application of machine vision in biosystems engineering. A computer vision method determined the distribution and amount of garlic, parsley, and vegetables ingredients in pasteurized cheese with an accuracy of over 88% compared with the sensory method (Jeliński et al., 2007). Morphometric features of three bread wheat varieties were quantified using a software employing artificial neural networks with 88% overall classification accuracy (Dubey et al., 2006). Visual inspection is the method currently used to determine seed size uniformity of soybean, but image analysis-based seed size measurements gave about 84% agreement by emulating the visual grading system (Shahin et al., 2006). This method predicted the size of soybean samples using linear discriminant function models and artificial neural network classifiers. A developed Visual Basic software simu-

* *Corresponding author*. Tel.: +1 662 325 3365; fax: +1 662 325 3853.
E-mail addresses: igathi@abe.msstate.edu; igathi@gmail.com (C. Igathinathane).
0168-1699/$ – see front matter © 2008 Elsevier B.V. All rights reserved.
doi:10.1016/j.compag.2008.02.007

lated planimeter manual tracing method of finding areas of irregular shapes and measured leaf area, dimensions, and perimeter (Igathinathane et al., 2006). Since an instrumental method was lacking to measure physically the bagasse fiber length and fineness, an image analysis method used electronic microscope to measure bagasse fiber length and fineness (Chiparus and Chen, 2003). A machine vision system algorithm classified appearance characteristics of different forms of rice (head, cracked, chalky, and broken), determined milling rate, identified whether the kernels were grouped or isolated, analyzed 200 kernels in 2 s, and found to be a satisfactory systems for inspection of appearance quality of rice with overall accuracy greater than 95% (Yun et al., 2002). A MATLAB algorithm performed leaf area measurement using either charge-coupled device camera or flat scanner acquired digital images that produced 100% leaf identification when there was no superposition between leaves (Li et al., 2007).

Quick and accurate particle size distribution analysis is desirable in various fields that handle granular or particulate materials. Particle size distribution analysis is considered as a standard procedure to evaluate the dimensional characteristics of a collection of particles in a sample. Standard results include geometric mean dimension, associated standard deviation, particles retained on different sieves, and cumulative size distribution curve. Size distribution of input feed material and output product material quantifies effectiveness of size reduction machinery. In turn, this can be related to the energy involved in the operation and the efficiencies of different size reduction machines. Although sieve analysis is the standard procedure of size distribution analysis of particles (ASABE Standards, 2006), computer vision-based image processing can be considered as an alternative or replacement method of analysis. Digital image processing was used for measuring dimensions and size distribution of circular particles (Momota et al., 1994), rock crusher aggregates (Maerz, 1998), coarse aggregates (Mora et al., 1998), and rain drops (Cruvinel et al., 1999).

Specific stand-alone user-coded computer vision applications of particle size and size distribution may require advanced programming using proprietary programming language environment such as Visual C, Visual Basic as well as MATLAB with specialized image processing toolboxes. Other methods can employ various morphological functions of commercial image processing software, such as Image Pro, National Instruments-Vision Builder, and EPIX-XCAP for morphological features extraction and quantification. An attractive alternative is ImageJ plugin development for particle size and size distribution as a machine vision application. ImageJ is a Java-based, multithreaded, freely available, open source, platform independent, and public domain image processing and analysis program developed at the National Institutes of Health (NIH), USA (Rasband, 2007; Bailer, 2006). ImageJ plugin is an executable Java code from ImageJ platform, tailor-made for a specific application including machine vision.

Most particle analysis software, including ImageJ, map the actual particle to an equivalent ellipse so that both area and perimeter matches. ImageJ has a built-in option for analyzing particles, which produces such output parameters as number of particles, areas, perimeters, and major and minor axes. Analysis using this technique although furnishes good estimates of area, perimeter, along with bounding rectangle dimension, best-fitted ellipse major axis, minor axis, and inclination of major axis, but does not provide the dimensions of practical interest such as length and width of the particles. Large deviations resulted when the available dimensions from the bounding rectangle's height and width were used to represent actual length and width of particles. This study establishes that fitted ellipse dimensions produce relatively good estimates; however, some deviations occurred from the actual dimensions of particles. Particle shapes also influenced the deviations. Therefore, fitted ellipse dimensions should be corrected for accurate particle dimension measurements with correction factors selectively applied after identifying the shapes of particles. Size distribution analysis of particles can be performed based on obtained length of particles. Thus this research work deals with the following objectives:

1. Development of an ImageJ plugin that determines the dimensions of particles by applying correction factors after identifying their shapes and analyzes the particle size distribution.
2. Determine the effects of shape, size, and orientation of geometric particles in dimensional measurements.
3. Demonstrate application of the plugin to actual examples of images of food grains and size reduced biomass particles.

2. Methods

2.1. *Background*

The binary image of any particle with continuous boundary can be modeled as an ellipse having equivalent area and perimeter of the particle. Distribution of the particle boundary coordinates after equating the second order central moments produces the best-fitting ellipse (Rodieck, 2007). Several other image analysis packages also use this second order central moment to fit the best ellipse and report the major and minor axes dimensions. Standard outputs of ImageJ relevant to particle sizing include area, perimeter, width and height of bounding rectangle, major and minor axes of best-fitting ellipse, angle of inclination of the major axis with the horizontal, and feret diameter. The feret diameter gives the maximum caliper dimension of the particle, but it represents the diagonal dimension rather than the length in case of rectangles. As shown later (Section 3.2), of the standard outputs, major and minor axes of the fitted ellipse best represented the actual length and width of the particle than the particle bounding rectangle's length and width. Hence, the proposed ImageJ plugin development deals only with major and minor axes of best-fitted ellipse, as a means of obtaining the actual dimensions.

Overestimation or underestimation of the actual length and width of some basic shapes of particles occurred, even though the ellipse fitting technique ensured the same area as well as perimeter of any particle shape (Fig. 1). This discrepancy from actual dimensions was highly pronounced only in the case of polygonal shapes with fewer numbers of sides, such as triangles, squares, and rectangles. Major and minor

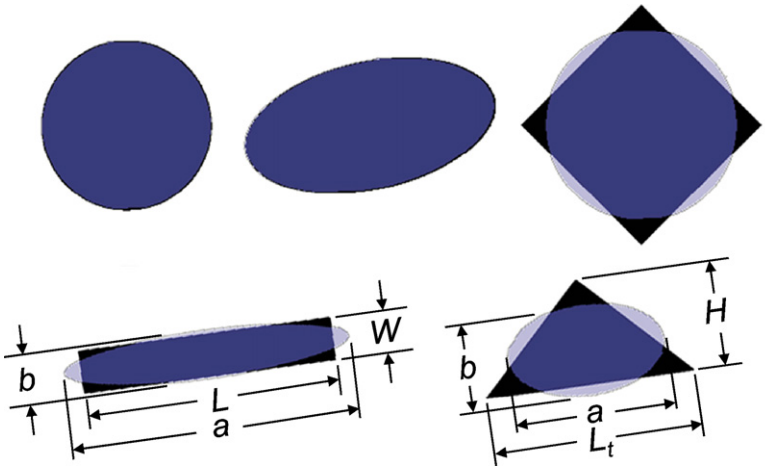

Fig. 1 – Dimension measurement anomaly observed in polygonal shaped particles. *a*, *b* is the major and minor axes of fitted ellipse; *L*, *W* is the length and width of rectangle shaped particles; L_t, *H* is the length of triangle shaped particle base and height.

axes dimensions of rectangular particles produce overestimation, while triangular particles produce underestimation. The deviation reduces when the outline profile approached smooth curves producing shapes such as circle or ellipse (Fig. 1).

Length of the particle is the decisive factor than the width while considering the particle's natural resting position as a criterion of retention on a sieve surface. Other parameters than length, namely width (smaller dimension), projected area, and perimeter will not have direct influence on the quantity of overflow or underflow material from a particular sieve. Therefore, determination of length is central for subjecting the particles through virtual set of sieves to simulate the standard sieve analysis using image processing.

2.2. *Particle dimension determination*

2.2.1. *Rectangular particles correction factor*

Appropriate correction factors can rectify the overestimation in dimension measurements of rectangular and square shapes. The area of particle was considered as the basis of comparison and correction factors evaluated, since area being a dominant property than perimeter as well as due to lack of exact analytical formula for ellipse perimeter. With usual notations, for a rectangular particle (Fig. 1), the actual length and width are determined as follows.

Let the area of the best-fitting ellipse for a rectangular object be

$$A_{ef} = \frac{\pi}{4}ab \tag{1}$$

where A_{ef} is the fitted area of ellipse representing a rectangular shape, a the major axis of ellipse, and b is the minor axis of ellipse ($a \geq b$). The actual area of the rectangular particle is given by

$$A_{ra} = LW \tag{2}$$

where A_{ra} is the actual area of rectangular particle, L the length of rectangle, and W is the width of rectangle ($L \geq W$). Assuming constant aspect ratio for both shapes, the ratios can be expressed as

$$\frac{L}{W} = \frac{a}{b} \tag{3}$$

Since both areas should match ($A_{ef} = A_{ra}$), equating Eq. (1) to Eq. (2) and eliminating W using Eq. (3) we arrive the rectangle length as

$$L = \frac{\sqrt{\pi}}{2}a \tag{4}$$

Similarly, eliminating L, the rectangle width is

$$W = \frac{\sqrt{\pi}}{2}b \tag{5}$$

Therefore, the constant correction factor ($\sqrt{\pi}/2 = 0.886227$) when applied to both major and minor axes (Eqs. (4) and (5)) will reduce the values, rectify the overestimation and thereby produce corrected length and width of actual rectangle. This correction factor is equally applicable for square shapes, since a square is a special case of rectangle with $L = W$.

2.2.2. *Triangular particles correction factor*

Unlike rectangles and squares, triangular particles did not have biaxial symmetry. Asymmetry exists with triangular particles about the major axis direction of fitted ellipse. The correction factor derivation strategy is similar to that of rectangular shapes, but involves specific correction factors for length and width, because of the asymmetry. The actual area of the triangular particle is expressed as

$$A_{ta} = \frac{1}{2}L_tH \tag{6}$$

where A_{ta} is the actual area of triangular particle, L_t the length of triangle base, and H is the height of triangle ($L_t \geq H$). Owing

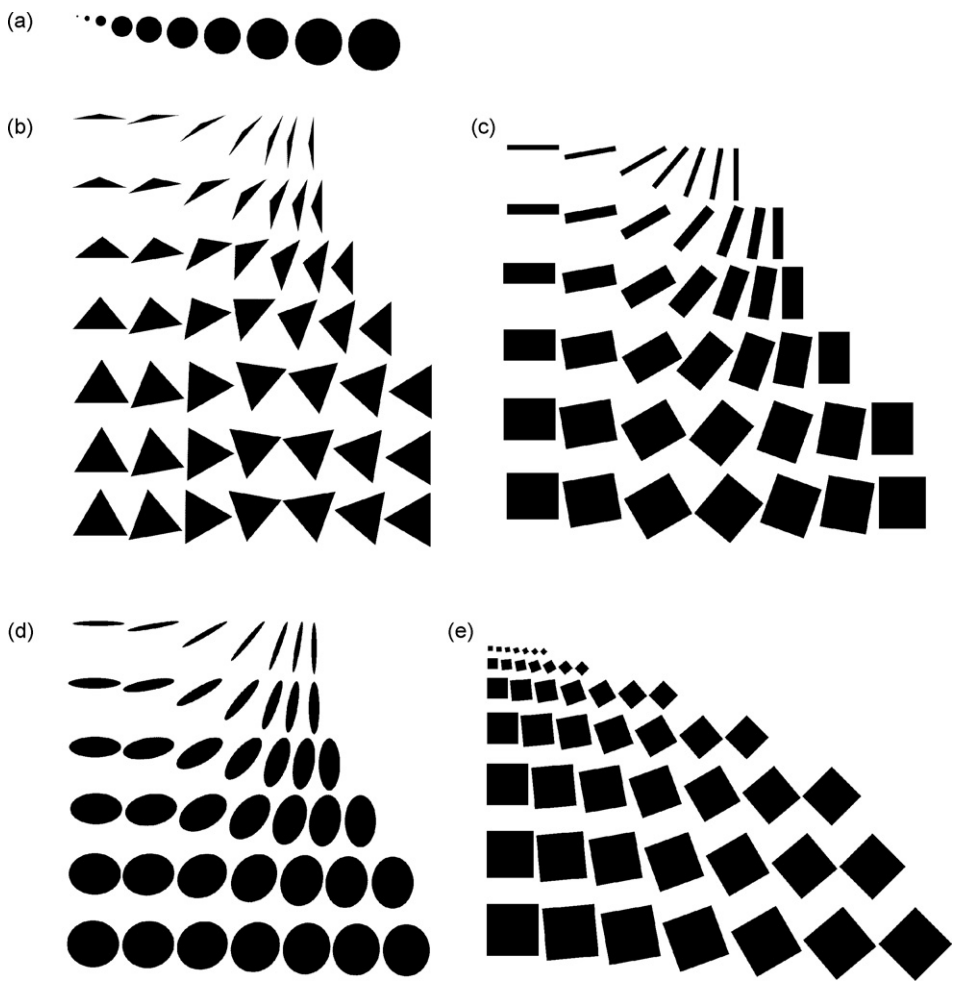

Fig. 2 – Drawn reference images of geometric shaped particles used in plugin development. (a) Circles with 10 different diameters: 5, 15, 30, 60, 75, 90, 105, 120, 135, and 150 pixel; (b) triangles; (c) rectangles; (d) ellipses—all these three shapes with length as 150 pixel, height or width by length ratios of 0.1, 0.2, 0.4, 0.6, 0.8, and 0.9 (instead of 0.9, triangles used 0.83 and 0.86), and orientation angles of 0°, 10°, 30°, 50°, 70°, 80°, and 90° combination; (e) squares with seven side dimensions: 15, 30, 60, 90, 120, 135, and 150 pixel, and orientation angles of 0°, 5°, 10°, 20°, 30°, 40°, and 45° combination.

to the asymmetry, the aspect ratios of triangle and ellipse were assumed to vary by a proportionality constant (C) as

$$\frac{L_t}{H} = C\frac{a}{b} \tag{7}$$

Equating Eq. (1) and Eq. (6) and eliminating the unknown variables in Eq. (7), the length of the triangle is

$$L_t = \left[\frac{C\pi}{2}\right]^{1/2} a \tag{8}$$

Correspondingly, the height of the triangle is

$$H = \left[\frac{\pi}{2C}\right]^{1/2} b \tag{9}$$

The mean C value was evaluated from reference triangle particles in various sizes and aspect ratios (Sections 2.3 and 3.1) as 1.157475 ± 0.006323. Therefore, the evaluated length $(C\pi/2)^{1/2}$ and width $(\pi/(2C))^{1/2}$ correction factors were 1.348391 and 1.164942, respectively. These specific correction factors (>1.0) when applied to respective major and minor axes (Eqs. (8) and (9)) will correct the observed underestimations and determine the actual length and height triangular particles.

2.2.3. *Ellipse particles correction factor*

Since any shape is fitted as an ellipse, it is natural that elliptical shapes will be fitted exactly matching the particle outline, with the major axis forming the length ($a = L$) and the minor axis the width ($b = W$) directly. The fitted ellipse automatically matches circular shape because circle is a special case of ellipse with major axis equals the minor axis ($a = b = L = W$). For ellipse and circular particles, actual outlines and best fitting ellipse outlines coincides exactly (Fig. 1), hence there is no need for correction or correction factor value is taken as 1.0.

2.3. *Reference particles*

Plugin development requires image of particles of known shapes and dimensions. Rather than working with actual

particle images of known shapes and dimensions, reference precision images were created by drawing various geometric shapes using ImageJ drawing tools. Drawings of circle, triangle, rectangle, ellipse, and square represented particles of various size, orientation, and height or width by length ratio (Fig. 2). An additional group of reference triangles evaluated the proportionality constant C. These triangles were drawn with a base of constant 150 pixels, orientation angles from 0° to 50° in steps of 5° and from 60° to 90° in steps of 10°, and each group having 15 triangles with 15 aspect ratios varying from 1.0 to 12.9 (total 225; not shown).

2.4. Shape identification

To extract the dimensional properties of the particles from the major and minor axes values, the correction factors need to be applied but their values depend on the geometric shapes that best represents the particle. Defining only three new shape parameters identified shapes from the ImageJ standard output properties of particles, such as area, perimeter, bounding rectangle dimensions, major and minor axes, inclination angle, and feret diameter, in a simplified manner. Of the several possible shape parameters, we defined the following three non-dimensional shape parameters in this study with usual notations:

$$\text{reciprocal aspect ratio,}\quad \text{RAR} = \frac{b}{a} \tag{10}$$

$$\text{rectangularity,}\quad \text{RTY} = \frac{A_{ef}}{H_b W_b} \tag{11}$$

$$\text{feret major axis ratio,}\quad \text{FMR} = \frac{D_f}{a} \tag{12}$$

where H_b is the height of bounding rectangle, W_b the width of bounding rectangle, and D_f is the feret diameter of fitted particle.

It is interesting to note that the common shape factors reported in literature such as roundness, compactness, circularity, area-perimeter ratio, and equivalent diameter were found not useful in identifying object shapes. In preliminary analysis with geometric shapes, the aforementioned shape factors failed to qualify as shape identifiers, but the three shape factors defined in this work (Eqs. (10)–(12)) singly or in combination of two, were able to classify the test shapes. The Java source code of the method implementing the shape identification to identify the eight different test shapes is presented in Appendix A. The length and width were evaluated as a product of respective major and minor axes, correction factors, and scale factor based on calibration procedure (Section 2.7). Implementation of this procedure is outlined in method source code given in Appendix B.

2.5. Image acquisition

The digital images were acquired using a flatbed scanner with 4800 dpi × 9600 dpi (Cano-scan 4400F, Canon U.S.A. Inc., Lake Success, NY). The test material was spread in single layer over a transparent sheet and placed on the scanner glass for imaging. For correct representation and measurement, the particles should be spread in a way that the particle neither overlap nor touch one another. For a better contrast, a black background was used while acquiring the images. The image was ultimately converted into binary form via 8-bit grey scale image before analysis.

2.6. Size distribution analysis

American Society of Agricultural and Biological Engineers (ASABE) standards (ANSI/ASAE S424.1, 2006) on determining and expressing particle size of feed and chopped forage materials by screening analyzed the particle size distribution and determined geometric mean length of particles. This standard method employed a set of sieves and measured the weight of materials retained on each sieve. With image processing method in this study, the number of particles retained on sieve equalized the weight of material. Comparison of the calculated dimensions of particles with selected sieve opening sizes obtained the number of particles retained on sieves. In the analysis we used the sieves opening side dimensions, rather than the diagonal opening dimension per ASABE standards, and considered the particle length as the working dimension. This assumption makes a particle of given length at any orientation angle will pass through a sieve of corresponding opening dimension, than considering diagonal opening dimension that only allows four possible orientations along diagonals. This approach can also be thought of having sieves of circular openings with only one dimension (diameter of opening) influencing the separation.

2.7. ImageJ plugin development

ImageJ plugin, even though a specialized limited code, has the advantage of inheriting all the functionality of ImageJ. The flowchart shows only the general steps involved in the plugin source code (Fig. 3). From the standard results, various processes, namely calculating the shape parameters, classifying the particles' shape (Section 2.3), finding linear dimensions of particles using correction factors (Section 2.2) based on shape classification, analyzing particle size distribution selecting a set of virtual sieves of standard dimensions (Section 2.5), and generating desired outputs are produced, as outlined in the flowchart (Fig. 3).

Considering the possibility of running the developed plugin in different computer systems and platforms, monitor resolutions, and usage of different image acquisition devices, a proper calibration of acquired image is imperative. The plugin accounts for these variation and extends its application through calibration procedure based on a few inputs from the user.

3. Results and discussion

3.1. Triangle proportionally constant

The C value, using the 225 triangle particles (Section 2.3; not shown) in various orientation angles and aspect ratios, varied from 1.15 to 1.20 with mean value of 1.157475 ± 0.006323. It can be seen that the mean C value was closer to minimum limit

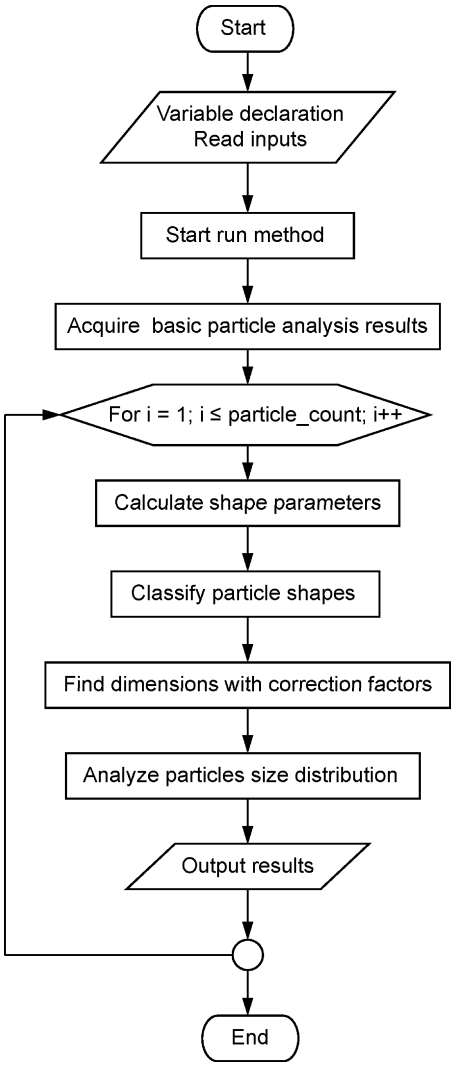

Fig. 3 – Flowchart of developed plugin to analyze particles size distribution based on dimensions.

and the small standard deviation value indicated close grouping. Hence, the single mean *C* value can be confidently used for all cases of triangles. The effect of this *C* value greater than unity in making the correction factors (Eqs. (8) and (9)) and correcting underestimation was already noted (Section 2.2.2).

3.2. *Dimensions representation discrepancy*

To assess the suitability of ImageJ in determining the dimensions of particles from the standard output options, rectangular particles in different sizes and orientations were considered for analysis. The reference image had three families of 10 rectangles each having different sizes at horizontal and 45° orientation, and Table 1 presents their actual dimensions, along with the plugin measured parameters and their analyzed deviations.

It can be seen from Table 1 that the ImageJ measurements with measured area (absolute values deviation% ± standard deviation%: 0.28 ± 0.51%) and perimeter (0.41 ± 0.33%) closely followed the actual values, because of its mechanism of matching the areas and perimeters. The image being composed of square matrix of pixels will have some differences in number of pixels that form a line segment. Also the inclined lines make the pixel arrangement look dithered while the 0° and 90° lines were smooth where pixels arranged side by side or one over the other (Igathinathane et al., 2006).

To represent the linear dimensions such as height and width, the options available in the standard measurements of ImageJ are bounding rectangle height and width, and the major and minor axes of the fitted ellipse. Although, bounding rectangle height and width represent the height and width of horizontally oriented particles exactly, the deviation becomes highly significant at 45° oriented particle. In addition, the bounding rectangle will always be a square, producing same dimensions for height and width, irrespective of the rectangle's aspect ratio when it is oriented at 45°. At other angles of orientation, one-dimension will be more affected than the other, based on whether the angle is greater or smaller than 45°. Therefore, bounding rectangle dimension cannot be considered as the choice for linear dimension measurements. Major and minor axes of fitted ellipse, based on their performance, make them the best available choice.

From the results of major and minor axes, the particles orientation inclination was observed to be no longer an issue. However, the calculated large percent mean absolute deviations of 12.77 ± 0.17% for major axis representing height, and 12.93 ± 0.66% for minor axis representing width, clearly demonstrate the dimension representation discrepancy as discussed earlier (Fig. 1). Using rectangle shape correction factor ($\sqrt{\pi}/2$; Eqs. (4) and (5)), these deviations were brought down to 0.09 ± 0.14% and 0.27 ± 0.52% for major axis representing height and minor axis for width, respectively.

Performing similar analysis with consideration of bounding rectangle's dimensions (Table 1) for particle's length and width produced enormous deviations. Percent deviation of bounding rectangle's width for actual length varied from −23.00% to 41.50%, while bounding rectangle's height for actual width varied from 0.00% to 675.00%. Mean absolute deviations of bounding rectangle's dimensions for actual length and width were 9.38 ± 13.44% and 127.10 ± 210.04%, respectively. This reveals the inadequacy of bounding rectangle dimension to represent actual particle dimension. It should also be mentioned that perfect measurements will result when the particles were oriented either horizontally or vertically irrespective of shape, but such orientations rarely occurs in practical scenario.

Triangular particles registered even more deviation than rectangular particles. From the analysis of the group of triangular particles (Fig. 2b), the major and minor axes produced percent mean absolute underestimations of 25.46 ± 0.28% for actual length and 14.17 ± 0.21% for actual height of triangles. Similarly bounding rectangle dimensions produced percent mean deviations of 5.47 ± 6.89% and 46.12 ± 99.58% for length and height, respectively. It is also obvious that circle and ellipse particles did not produce significant deviations.

Hence, it is clear that the dimension of fitted ellipse is a better option than the bounding rectangle for dimensions. Even though ImageJ had reduced deviation (≤0.41%) with areas and perimeters, it produced significant deviation (≤12.93%) from fitted ellipse's major and minor axes taken as actual

Table 1 – ImageJ measurement results for rectangular objects in different sizes and orientations

Particle number	Actual height (pixel)	Actual width (pixel)	Actual area (pixel^2)	Actual perimeter (pixel)	Measured area (pixel^2)	Measured perimeter (pixel)	Bounding height (pixel)	Bounding width (pixel)	Major axis (pixel)	Minor axis (pixel)	Deviation area (%)	Deviation perimeter (%)	Deviation major axis[a] (%)	Deviation minor axis[a] (%)
1	100	10	1,000	220	1,000	217.66	10	100	112.84	11.28	0.00	−1.06	12.84	12.80
2	100	20	2,000	240	2,000	237.66	20	100	112.84	22.57	0.00	−0.98	12.84	12.85
3	100	40	4,000	280	4,000	277.66	40	100	112.84	45.14	0.00	−0.84	12.84	12.85
4	100	60	6,000	320	6,000	317.66	60	100	112.84	67.70	0.00	−0.73	12.84	12.83
5	100	100	10,000	400	10,000	397.66	100	100	112.84	112.84	0.00	−0.58	12.84	12.84
6	100	10	1,000	220	987	217.79	77	77	112.31	11.19	−1.30	−1.00	12.31	11.90
7	100	20	2,000	240	2,044	237.59	84	84	112.41	23.15	2.20	−1.00	12.41	15.75
8	100	40	4,000	280	4,018	277.19	98	98	112.43	45.50	0.45	−1.00	12.43	13.75
9	100	60	6,000	320	5,993	319.61	113	113	112.44	67.86	−0.12	−0.12	12.44	13.10
10	100	100	10,000	400	9,941	398.81	141	141	112.50	112.50	−0.59	−0.30	12.50	12.50
11	200	20	4,000	440	4,000	437.66	20	200	225.68	22.57	0.00	−0.53	12.84	12.85
12	200	40	8,000	480	8,000	477.66	40	200	225.68	45.14	0.00	−0.49	12.84	12.85
13	200	80	16,000	560	16,000	557.66	80	200	225.68	90.27	0.00	−0.42	12.84	12.84
14	200	120	24,000	640	24,000	637.66	120	200	225.68	135.41	0.00	−0.37	12.84	12.84
15	200	200	40,000	800	40,000	797.66	200	200	225.68	225.68	0.00	−0.29	12.84	12.84
16	200	20	4,000	440	3,962	438.41	155	155	225.35	22.39	−0.95	−0.36	12.68	11.95
17	200	40	8,000	480	7,924	478.00	169	169	225.39	44.76	−0.95	−0.42	12.70	11.90
18	200	80	16,000	560	15,990	560.03	198	198	225.37	90.34	−0.06	0.01	12.69	12.93
19	200	120	24,000	640	24,054	638.40	226	225	225.80	135.64	0.23	−0.25	12.90	13.03
20	200	200	40,000	800	40,044	799.62	283	282	225.81	225.79	0.11	−0.05	12.91	12.90
21	400	40	16,000	880	16,000	877.66	40	400	451.35	45.14	0.00	−0.27	12.84	12.85
22	400	80	32,000	960	32,000	957.66	80	400	451.35	90.27	0.00	−0.24	12.84	12.84
23	400	160	64,000	1120	64,000	1117.66	160	400	451.35	180.54	0.00	−0.21	12.84	12.84
24	400	240	96,000	1280	96,000	1277.66	240	400	451.35	270.81	0.00	−0.18	12.84	12.84
25	400	400	160,000	1600	160,000	1597.66	400	400	451.35	451.35	0.00	−0.15	12.84	12.84
26	400	40	16,000	880	16,130	878.23	310	311	451.55	45.48	0.81	−0.20	12.89	13.70
27	400	80	32,000	960	31,979	958.84	339	339	451.59	90.16	−0.07	−0.12	12.90	12.70
28	400	160	64,000	1120	64,240	1119.23	395	396	451.60	181.12	0.38	−0.07	12.90	13.20
29	400	240	96,000	1280	96,219	1279.03	452	452	451.60	271.28	0.23	−0.08	12.90	13.03
30	400	400	160,000	1600	160,177	1598.65	565	565	451.60	451.60	0.11	−0.08	12.90	12.90
Mean[b]											0.28	0.41	12.77	12.93
S.D.[b]											0.51	0.33	0.17	0.66

Particle numbers 6–10, 16–20, and 26–30 are oriented with the major dimension at an angle of 45° counter clockwise from horizontal.

[a] Based on respective actual height and width.

[b] Based on absolute values.

Table 2 – Particle shape parameter values used in the strategy of shape identification

Shape	RAR	RTY	FMR
Circle	1.000–1.000	0.750–0.889	1.009–1.144
Triangle	0.115–0.991	0.110–0.517	1.295–1.351
Rectangle-straight	0.100–0.900	1.000–1.000	0.891–1.192
Rectangle-inclined	0.100–0.900	0.170–0.750	0.895–1.195
Ellipse-straight	0.102–0.900	0.780–0.788	0.999–1.007
Ellipse-inclined	0.102–0.900	0.160–0.780	1.002–1.010
Square-straight	1.000–1.000	1.000–1.000	1.253–1.253
Square-inclined	0.970–1.000	0.500–0.879	1.235–1.262

RAR: reciprocal aspect ratio (Eq. (10)); RTY: rectangularity (Eq. (11)); FMR: feret major axis ratio (Eq. (12)).

length and width, respectively. Therefore, it is realized that shape-based correction factors to fitted ellipse dimensions are essential for measurement of linear dimensions.

3.3. *Shape parameters of particles of geometric shapes*

Running the plugin with individual shape groups to determine their deviation spread among shapes evaluated shape parameter values of geometric particle drawing images (Fig. 2) using Eqs. (10)–(12) (Table 2). The dimensionless shape parameters RAR and RTY varied from 0.1 to 1.0, while FMR varied from 0.89 to 1.35 based on their definition across different shapes.

Shape parameter RAR indicated flatness of the shape and for circle and straight squares its value is 1. This can be used to identify circles and straight squares. Shape parameter RTY was based on how much portion of the bounding rectangle of region of interest (ROI) got filled by particle area; thereby producing a value of 1 for straight rectangles and squares, and other shapes producing values less than 1. Triangle shapes had the least filling of the bounding rectangle (RTY = 0.11–0.52), whereas circles had partial filling but producing a fixed range (RTY = 0.75–0.89). Shape factor FMR naturally produces values closer to one when the object shapes are circle, and straight and inclined ellipses (1.00–1.14). Larger values of FMR observed (Table 2) with circle were because of circles of smallest diameter (e.g., 1.14; 4 pixel wide) to be represented by a grid of square pixels. Whereas, the FMR value for 15 pixel diameter circle was reduced to 1.05, and FMR value reduced further with increase in circle diameter. It is interesting to note that for triangle shapes the FMR values stand apart (1.30–1.35) from other shapes allowing for easy identification. These observations of the shape parameter ranges, their combination, and other values obtained from preliminary runs, led to the development of shape identification strategy employed in this work (Appendix A).

3.4. *Shape identification and dimension measurements*

An image, of a group of known geometric shapes and dimensions, was drawn and tested (Fig. 4) for shape identification and dimensions measurements, and the results obtained are presented in Table 3. Length and width of particles expressed in the basic units of pixels can be converted into any physical unit after working out a scale

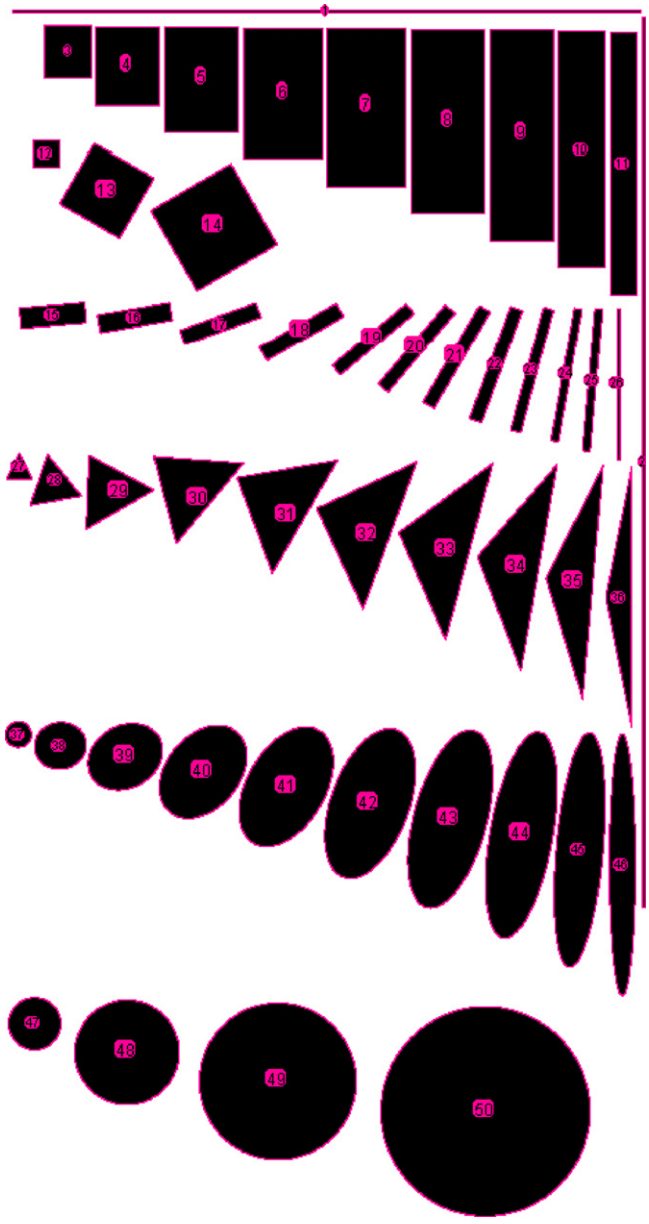

Fig. 4 – Test particles of different geometric shapes showing labels and fitted profiles.

factor from the calibration procedure. The correctness of the determined dimensions can be easily checked by recalculating the area and perimeter values of ImageJ outputs, which were accurate as demonstrated earlier (Table 1). Mean percent absolute deviation of areas of all the 50 particles calculated again from the determined dimensions was only $0.0007 \pm 0.001\%$ from the actual areas proving the accuracy of the plugin. However, the mean absolute deviation of perimeters of all particles, with ellipse perimeter evaluated by Ramanujan I approximation (Sýkora, 2005), was $4.4 \pm 3.1\%$. This increased deviation stems from the fact that the correction factors were derived based on areas (not perimeters) by equating actual areas and fitted ellipse dimensions (Section 2.2). This deviation of this calculated perimeter is of

Table 3 – Shape identification and dimension determination using correction factors of different particle shapes

Count	Angle (°)	Area (pixel^2)	Perimeter (pixel)	RAR	RTY	FMR	Particle shape	Length (pixel)	Width (pixel)
1	0	125,189	10929.7	0.004	1.000	0.886	Rectangle-straight	5443.0	23.0
2	90	177,330	15463.7	0.003	1.000	0.886	Rectangle-straight	7710.0	23.0
3	90	185,232	1721.7	0.899	1.000	1.192	Rectangle-straight	454.0	408.0
4	90	369,920	2445.7	0.800	1.000	1.135	Rectangle-straight	680.0	544.0
5	90	575,945	3081.7	0.700	1.000	1.082	Rectangle-straight	907.0	635.0
6	90	771,120	3625.7	0.600	1.000	1.033	Rectangle-straight	1134.0	680.0
7	90	925,480	4079.7	0.500	1.000	0.991	Rectangle-straight	1361.0	680.0
8	90	1,007,745	4441.7	0.400	1.000	0.955	Rectangle-straight	1587.0	635.0
9	90	986,816	4713.7	0.300	1.000	0.925	Rectangle-straight	1814.0	544.0
10	90	832,728	4895.7	0.200	1.000	0.904	Rectangle-straight	2041.0	408.0
11	90	514,836	4987.7	0.100	1.000	0.891	Rectangle-straight	2268.0	227.0
12	0	51,529	905.7	1.000	1.000	1.253	Square-straight	227.0	227.0
13	106	360,019	2572.5	1.000	0.537	1.253	Square-inclined	600.0	600.0
14	165	646,442	3448.1	1.000	0.537	1.253	Square-inclined	804.0	804.0
15	5	102,677	1542.9	0.319	0.768	0.931	Rectangle-inclined	567.1	181.1
16	10	101,051	1676.0	0.251	0.580	0.914	Rectangle-inclined	635.1	159.1
17	20	95,720	1812.6	0.194	0.368	0.903	Rectangle-inclined	703.1	136.1
18	30	104,931	1943.3	0.176	0.284	0.900	Rectangle-inclined	771.1	136.1
19	40	94,897	1963.0	0.135	0.212	0.895	Rectangle-inclined	839.1	113.1
20	50	102,571	2104.0	0.125	0.200	0.894	Rectangle-inclined	907.1	113.1
21	60	110,301	2333.5	0.116	0.209	0.893	Rectangle-inclined	975.1	113.1
22	70	117,989	2497.7	0.108	0.250	0.892	Rectangle-inclined	1043.1	113.1
23	75	101,252	2578.5	0.082	0.246	0.890	Rectangle-inclined	1111.1	91.1
24	80	80,317	2631.8	0.058	0.253	0.888	Rectangle-inclined	1179.0	68.1
25	85	84,958	2711.5	0.055	0.387	0.888	Rectangle-inclined	1247.0	68.1
26	90	30,245	2673.7	0.017	1.000	0.886	Rectangle-straight	1315.0	23.0
27	90	25,651	769.9	0.866	0.502	1.303	Triangle	261.9	195.9
28	100	92,665	1463.9	0.962	0.472	1.334	Triangle	472.2	392.5
29	30	185,305	2070.5	0.924	0.491	1.347	Triangle	681.5	543.8
30	50	287,582	2569.7	0.807	0.492	1.346	Triangle	908.2	633.3
31	60	385,618	3107.6	0.693	0.450	1.347	Triangle	1135.3	679.3
32	70	462,350	3548.5	0.577	0.416	1.346	Triangle	1362.2	678.9
33	75	504,184	3867.6	0.462	0.402	1.345	Triangle	1589.7	634.3
34	80	493,890	4143.5	0.346	0.399	1.345	Triangle	1816.5	543.8
35	85	416,916	4469.5	0.231	0.415	1.344	Triangle	2044.1	407.9
36	90	256,303	4706.6	0.115	0.502	1.344	Triangle	2267.0	226.1
37	0	40,108	747.0	0.983	0.785	1.004	Ellipse-straight	228.0	224.0
38	10	145,473	1428.4	0.900	0.783	1.002	Ellipse-inclined	453.7	408.3
39	30	290,914	2034.1	0.800	0.772	1.002	Ellipse-inclined	680.5	544.3
40	50	452,554	2574.1	0.700	0.740	1.001	Ellipse-inclined	907.3	635.1
41	60	606,051	3052.7	0.600	0.713	1.001	Ellipse-inclined	1134.0	680.5
42	70	727,274	3477.6	0.500	0.708	1.001	Ellipse-inclined	1360.8	680.5
43	75	791,933	3857.9	0.400	0.695	1.001	Ellipse-inclined	1587.6	635.1
44	80	775,871	4192.9	0.300	0.697	1.000	Ellipse-inclined	1814.5	544.4
45	85	654,681	4484.1	0.200	0.723	1.000	Ellipse-inclined	2041.6	408.3
46	90	404,314	4735.8	0.100	0.785	1.000	Ellipse-straight	2268.3	227.0
47	173	161,633	1502.6	1.000	0.784	1.003	Circle	453.7	453.6
48	8	646,489	3004.7	1.000	0.786	1.002	Circle	907.3	907.2
49	5	1,454,492	4507.1	1.000	0.786	1.001	Circle	1360.9	1360.8
50	171	2,585,737	6010.6	1.000	0.786	1.001	Circle	1814.5	1814.4

less concern, as we are interested only in determining the dimensions of particles, and the areas and perimeters can be anyhow directly obtained from the standard ImageJ output.

It was observed that when the particles were minute and represented only by a few pixels, some misclassification occurred with other samples. In the strict sense, a very minute particle of any shape smaller than the dimensions of the pixel element can only be represented by a straight square in the image. Similarly when the particle size increased to a few pixels, visibly distinctive shapes cannot be drawn that in turn produced shape misclassification by the plugin. There was always a chance of shapes misclassification, as these limiting ranges of defined shape parameters were arrived only from test images of geometric shapes (Fig. 2) and the simplified strategy was based on only a few shape parameters. The possible limiting factors contributing to misclassification are (1) overlapping shape parameters values, (2) grid of square pixels

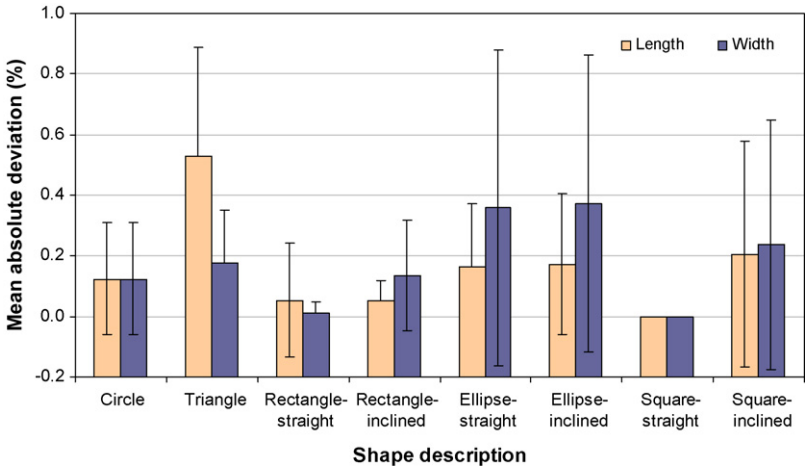

Fig. 5 – Mean absolute deviation of length and width measurements of different particle shapes.

representing particles of curved outlines especially when the area was minute, (3) irregular shapes that do not conform or deviate from the test cases, and (4) physical overlapping and touching particles during image acquisition. Machine vision works generally encounters these limitations and proceeds with simplifying assumptions. Avoiding such misclassification actually requires further research to find the regions of overlaps and to create a catalog of critical images that are likely to be misclassified.

3.5. *Effect of shape, size, and orientation of particles*

Effect of particle shapes in determining the length and width was determined using the geometric reference particles (Fig. 2) through mean absolute deviation from the actual dimensions (Fig. 5). Mean absolute deviations of length were less than 0.2% for all other shapes studied, except for triangle (0.5%). Mean absolute deviations of width were less than 0.4% for all shapes. Straight squares produced 0.0% deviation on both

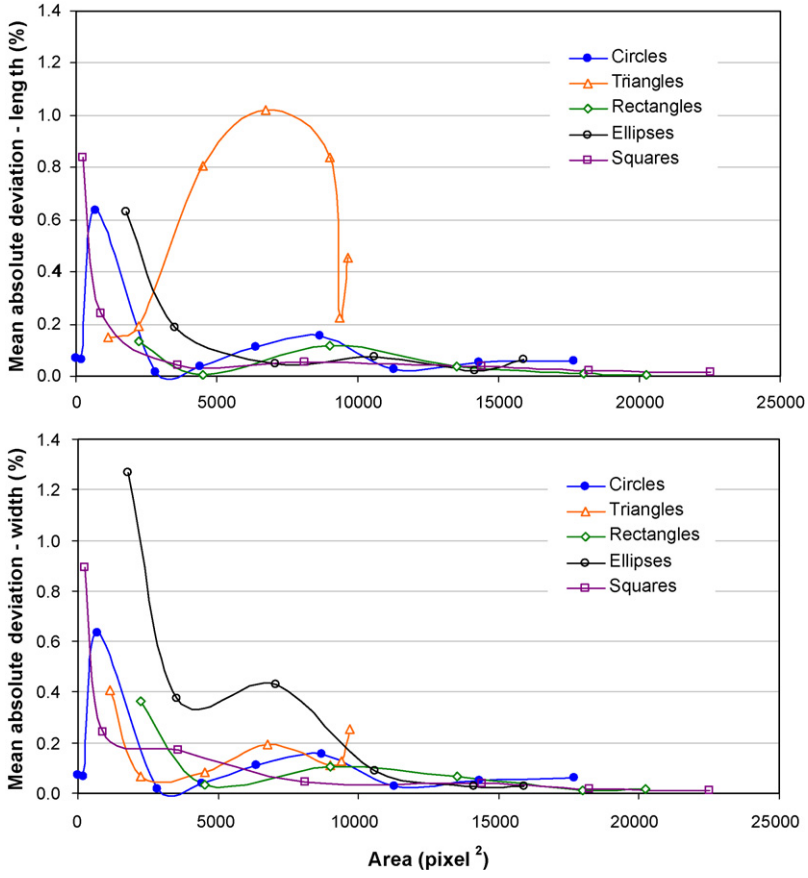

Fig. 6 – Mean absolute deviation of length and width measurements showing effect of area of different particle shapes.

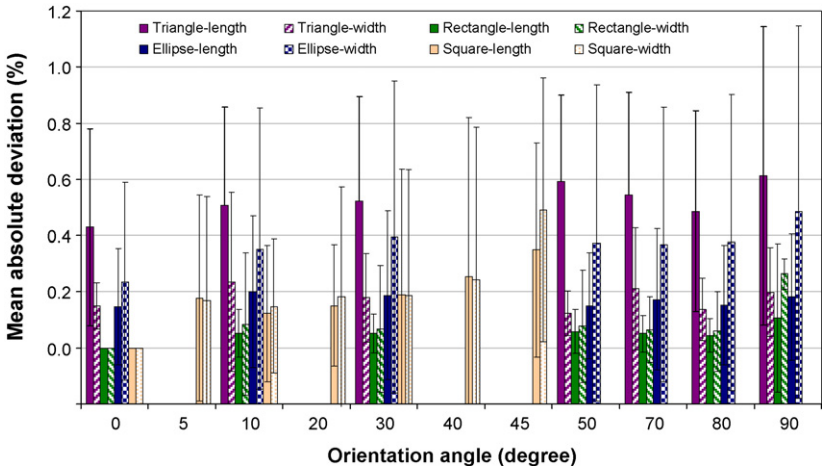

Fig. 7 – Mean absolute deviation of length and width measurements showing effect of orientation angle of different particle shapes.

length and width. Except for triangles and straight rectangles, width deviated more than the length because of comparative smaller values. Thus, the application of correction factors demonstrates effective handling of shapes with a small mean absolute deviation of <0.5% for length and width, and the deviation of <0.9% including data variation across shapes studied.

Effect of areas in determining the length and width of different shapes (Fig. 6) shows that mean absolute deviation of lengths were relatively smaller than the widths. The deviations tend to decrease with increase in area, as particles are better represented with increased areas. As observed earlier, lengths of triangles and widths of ellipses produced increased deviation. Except for triangle length, the absolute mean deviations of length and width above 5000 pixel^2 area (≈36 mm^2) were <0.2%.

Effect of particle orientation of various shapes in terms mean absolute deviation shows no great variation among various angles (Fig. 7). Absence of variation and small values of mean absolute deviation (<0.6%) establishes the superior capabilities of ImageJ in handling particles at any orientation angle. Within the small range of variation, the deviation gradually increased with increased orientation angles. Among shapes, in general, width produced more deviation than lengths except for triangles. The orientation angle effect of square particles shows a steady increase in mean absolute deviation from 0.0% to 0.5% when angle increased from 0° to 45°, but the mean absolute deviation range was narrow. Since

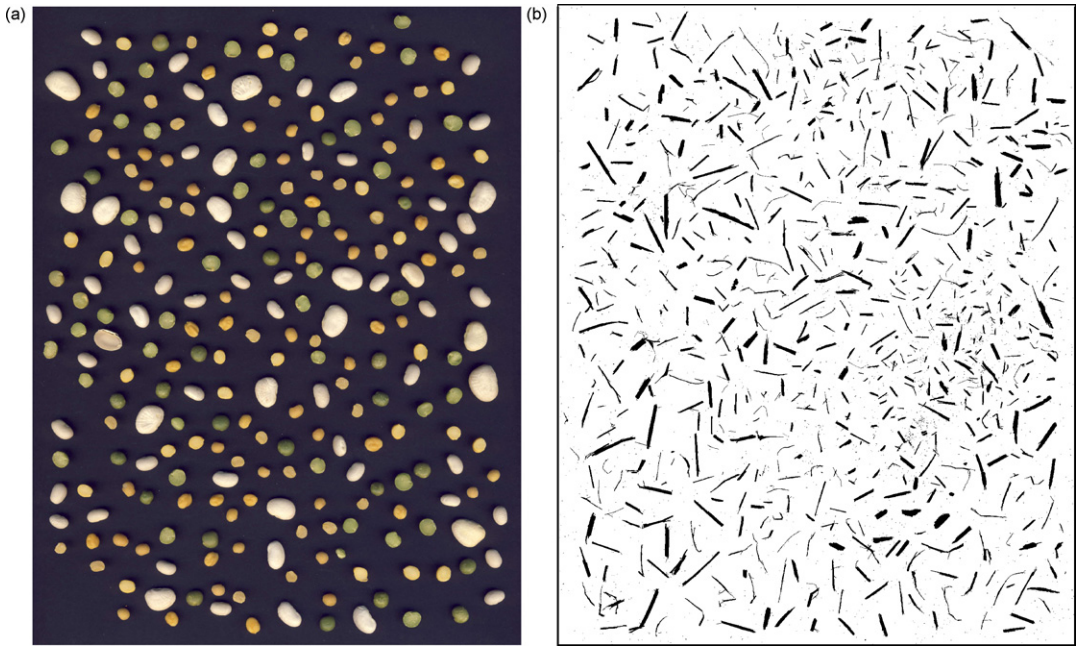

Fig. 8 – Images of actual particles used in the analysis. (a) Original color image of some whole and split beans (2324 pixel × 3140 pixel; 300 dpi); (b) 8-bit binary image mask of hammer-milled dry Miscanthus biomass with particles of area from 4 pixel^2 upwards (2456 pixel × 3144 pixel; 300 dpi).

Table 4 – Size distribution results summary of food grains and Miscanthus biomass particles

Material	Length (mm)[a]			Width (mm)			Length (mm)[b]	
	Min.	Max.	Mean ± S.D.	Min.	Max.	Mean ± S.D.	X_{gm}	S_{gm}
Food grains	4.72	15.67	7.41 ± 2.17	3.45	11.73	5.81 ± 1.34	6.43	1.53
Miscanthus	0.28	22.93	5.03 ± 4.18	0.08	4.94	0.84 ± 0.65	3.58	2.39

[a] Min.: minimum dimension; Max.: maximum dimension; Mean ± S.D.: arithmetic mean ± standard deviation.
[b] ASABE Standards (2006) was used to find the geometric mean length (X_{gm}) and standard deviation on geometric mean length (S_{gm}).

square's length and width are actually equal, no clear trend in mean absolute deviation was observed. The mean absolute deviation, including the data variation from the mean, was observed to be less than 1.2% for all shapes, dimensions, and orientation angles tested.

Overall, it can be concluded that shape is not having any effect on mean absolute deviation; increased area reduced the mean absolute deviation; orientation angle did not have major variation but showed a gradual increasing trend with orientation angle.

3.6. *Size distribution analysis with food grain*

During calibration on a 17″ monitor, a reference image of a rectangle 200 mm width × 260 mm height was measured as 2354.67 pixel × 3065.50 pixel. This gave the single pixel dimensions as 0.084938 mm × 0.084815 mm, making the horizontal by vertical ratio as 1.001447. Since the ratio was very close to a value of 1.0, each pixel can be considered virtually as a square. A mean value of 0.0848762337 mm/pixel was used as the scale factor value for dimensions conversion. The plugin after calibration processed the image of food grains containing whole and split beans (Fig. 8a). Classification results of the total 258 particles count were: circle = 1 (0.4%), ellipse-inclined = 251 (97.3%), ellipse-straight = 3 (1.2%), rectangle-inclined = 3 (1.2%), and unclassified = 0 (0.0%).

These results indicate the very good shape classification efficiency of the developed plugin with round particles that includes circles and ellipses. Interestingly, one perfect circle was found that can be easily located in the image with the existing labeling feature of ImageJ and by also using "ROI Manager" option. Random spot checks on dimensions of grains using digital vernier calipers helped comparing the image analysis results. A total of 40 grains (10 grains × 4 types) recorded percent mean absolute deviations of 2.59 ± 2.24% for length and 2.85 ± 2.37% for width. The observed deviations were better than the accuracies of reported various computer vision applications (95%, Yun et al., 2002; 88%, Dubey et al., 2006; 84%, Shahin et al., 2006; 88%, Jeliński et al., 2007). A summary of measured dimensions, their range, arithmetic mean and standard deviation, and geometric mean length (significant output of sieve separation analysis) and corresponding standard deviation (ASABE Standards, 2006) based on particles retained on 10 virtual sieves equally spaced between the minimum and maximum length spread, and the eleventh sieve acting as pan is presented in Table 4.

Spread of length values was only slightly greater than that of the width, as the particles were more of round or elliptical shape with mean RAR value was about 0.80, also reflected from the mean widths and lengths. Arithmetic mean length (7.41 ± 2.17 mm) tends to coincide with the geometric mean length (6.43 ± 1.53 mm). Particle size distribution characteristics of grain particle retained on 10 sieves plus pan shows a maximum number of particles on second sieve from bottom (Fig. 9). Although in the particle distribution, more particles were retained on sieves of

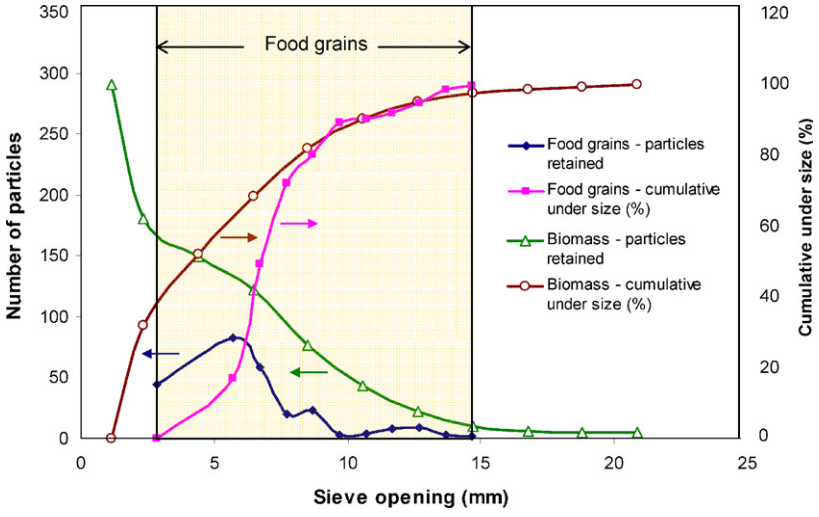

Fig. 9 – Size distribution particles retained on sieves and cumulative under size results of whole and split grains and Miscanthus biomass particles based on 10 equally spaced hypothetical sieves plus pan selected from the length dimensions spread using image analysis.

smaller openings, a peak resembling the hypothetical normal distribution "dumbbell" shaped curve was seen towards the left. This relative tendency towards the normal distribution might explain the observed coincidence of the arithmetic and geometric mean lengths. The cumulative under size curve showed steep increase because the spread of length was relatively small. The computation time taken for the complete analysis of the food grains image was 0.92 ± 0.01 s for a computer system with Intel Pentium 4 (CPU 3.00 GHz; 1.99 GB RAM) processor, based on system's internal clock.

3.7. *Size distribution analysis with ground biomass*

The plugin processed the image of hammer-milled dry Miscanthus biomass particles, counted 910 particles, and identified particle shapes (Fig. 8b) as follows: triangle = 233 (25.6%), rectangle-straight = 5 (0.5%), ellipse-inclined = 283 (31.1%), ellipse-straight = 6 (0.7%), rectangle-inclined = 383 (42.1%), and unclassified = 0 (0.0%). A bent particle like an arc or a particle approximately forming two sides of a triangle is classified as triangle shape, even though it only forms the two legs of the triangle with non-existing base. Ideally, these particles are two rectangles with radiating axes from the point of sharp bend, but the shape classification strategy (Appendix A) does not have provision to check for all the three sides and correctly classify as triangles. Advanced classification strategies or alternative methods need to be evolved to address this issue, which require further research.

Miscanthus biomass particles exhibit a wider spread on length and narrower spread on width (Table 4). This indicates that the particles were slender and rod-like, which was evident from the reduced value of calculated mean RAR as 0.26. A clear difference between the arithmetic mean length (5.03 ± 4.18 mm) and the geometric mean length (3.51 ± 2.39 mm) is observed. Size distribution curve of particles retained on sieves (Fig. 9) indicates only the right leg of the hypothetical normal distribution curve, unlike that observed with food grains. A large retention of particles (742 out of 910 = 81.5%) on the bottom three sieves including the pan caused the observed shift in the distribution. The geometric mean took into account the observed distribution and shifted the mean towards the smaller length particles. This constituted a better representation of the length of sample population. The arithmetic mean gave equal weight to all particles and shifted the mean towards the right creating the observed difference between the two means. Based on this observed distribution of particles on sieves, it is possible to rework the analysis by selecting more number of sieves, so that finer particles will be better distributed on an increased number of sieves. Ground Miscanthus image took a computation time of 1.89 ± 0.04 s. Computation speed varied inversely with the area of the particle. Based on the two images studied, the number of particles that can be analyzed per second was 279 ± 4.4 and 481 ± 10.6 for food grains and ground Miscanthus, respectively.

It should be mentioned that the particles retained on the sieves were strictly mathematically allocated based on their length. In practical mechanical sieving operations, particles will bounce off the sieve surface and sometimes pass through sieve openings widthwise, even though sieve openings are smaller than the particle's length. Therefore, this deviation cannot be construed as a drawback of image processing method of size distribution analysis, but to be attributed only to separation efficiency of mechanical system. This research indicates a great potential for developing ImageJ plugins to provide tailor-made solutions giving rapid analysis to suit specific needs of machine vision applications.

4. Conclusions

An ImageJ image processing plugin to determine dimensions of particles and their size distribution was successfully developed through shape identification and application of derived correction factors. Dimension representation anomaly of using major and minor axes to represent length and width produced significant overestimation (≈13%) with square and rectangular shapes, and underestimation with triangular shapes length (≈25%) and height (≈14%). Notwithstanding the observed deviations, it was clearly established that dimensions of fitted ellipse are the better option for dimensions measurement than dimensions of bounding rectangle. Three defined shape parameters, such as reciprocal aspect ratio, rectangularity, and feret major axis ratio, and their combination identified particles into eight basic geometric shapes (circle, triangle, rectangle straight and inclined, ellipse straight and inclined, and square straight and inclined). Particle shapes variation did not affect the determined dimensions (<0.5% mean absolute deviation). Effect of size in terms of particle areas mean absolute deviations (<1.3%) in general reduced as the particle area increased. Effect of particle orientation angle from 0° to 90° did not have any major effect (<0.6% mean absolute deviation); however, an overall increasing trend of deviation was observed with increasing orientation angle. The developed plugin was successfully applied in analyzing the actual images of food grains and hammer-milled dry Miscanthus biomass particles for dimensions and size distribution. Size distribution analysis showed that food grains and ground Miscanthus biomass distributions deviated from normal distributions, and the arithmetic and the geometric mean lengths were similar for food grains but different for biomass particles. This image processing plugin can be applied to rapid dimension measurements and particle size distribution analysis of various particulate systems from a digital image of disjoint particles.

Acknowledgements

Profound thanks are due to Ms. Maureen Smith, Computer Applications Training Officer, Stokely Management Center, The University of Tennessee, for the introduction to ImageJ. Thanks are due to William Massey, undergraduate student, Agricultural and Biological Engineering Department, Mississippi State University (MSU), for the work in this investigation. The Sustainable Energy Research Center, MSU, supported this research. This support is gratefully appreciated.

Appendix A

```
void classifyObjects() {
int numbers = areas.length;
classi = new String[numbers];
for (int i = 0; i < counter; i++) {
      classi[i] = "Random";
      if ((RTY[i] <= 0.6) && (FMR[i] >= 1.27))
            {classi[i] = "Triangle"; nt++; continue;}
      if ((RAR[i] >= 0.98) && (RTY[i] >= 0.98))
            {classi[i] = "Square-straight"; nss++; continue;}
      if ((RAR[i] >= 0.97) && (FMR[i] >= 1.2))
            {classi[i] = "Square-inclined"; nsi++; continue;}
      if ((RAR[i] < 0.98) && (RTY[i] >= 0.98))
            {classi[i] = "Rectangle-straight"; nrs++; continue;}
      if ((RAR[i] >= 0.99) && ((FMR[i] > 0.995 ) && (FMR[i] <= 1.15)))
            {classi[i] = "Circle"; nc++; continue;}
      if ((FMR[i] >= 0.98) && (FMR[i] <= 1.09))
            if(((angle[i]>=1)&&(angle[i]<=89))||((angle[i]>=91)&&(angle[i]<=179)))
                  {classi[i] = "Ellipse-inclined"; nei++; continue;}
            else  {classi[i] = "Ellipse-straight"; nes++; continue;}
      if ((FMR[i] < 0.98) || (FMR[i] > 1.09))
      {classi[i] = "Rectangle-inclined"; nri++; continue;}
      } // for loop
} // classifyParticles method
```

Appendix B

```
void evaluateDimensions() {
int numbers = particle_count;       float C = (float) 1.157475;
Length = new float[numbers];
Width = new float[numbers];
for (int i = 0; i < counter; i++) {
      shapeType = classi[i];  shapes = 0;
      correctionFactor = (float) (0.0);
      if (shapeType == "Ellipse-straight" || shapeType == "Ellipse-inclined"
            || shapeType == "Circle") shapes =  1; // "ellipse"
      if (shapeType == "Rectangle-straight" || shapeType == "Rectangle-inclined"
            || shapeType == "Square-straight" || shapeType == "Square-inclined")
            shapes =  2; // "rectangle"
      if (shapeType == "Triangle")
            shapes =  3; // "triangle"
      switch(shapes) {
            case 1:
                  corFactL = corFactW = (float) (1.0); break;
            case 2:
                  corFactL = corFactW = (float) (Math.sqrt(Math.PI)/2); break;
            case 3:
                  corFactL = (float) (Math.sqrt((C*Math.PI/2)));
                  corFactW = (float) (Math.sqrt((Math.PI/(2*C)))); break;
            } // switch
      Length[i] = majAxis[i]*corFactL*scaleFactor;
      Width[i] = minAxis[i]*corFactW*scaleFactor;
      } // for loop
} // evaluateDimensions method
```

REFERENCES

ASABE Standards, 2006. Method of Determining and Expressing Particle Size of Chopped Forage Materials by Screening—ANSI/ASAE S424.1 DEC01. ASABE, St. Joseph, Michigan, pp. 619–621.

Bailer, W., 2006. Writing ImageJ Plugins—A Tutorial. Version 1.71. http://rsb.info.nih.gov/ij/download/docs/tutorial171.pdf (Accessed February 2008).

Chiparus, O., Chen, Y., 2003. An image method to evaluate bagasse fiber dimensions. Bioresour. Technol. 90, 305–309.

Cruvinel, P.E., Vieira, S.R., Crestana, S., Minatel, E.R., Mucheroni, M.L., Neto, A.T., 1999. Image processing in automated

measurements of raindrop size and distribution. Comput. Electron. Agric. 23, 205–217.
Dubey, B., Bhagwat, S., Shouche, S., Sainis, J., 2006. Potential of artificial neural networks in varietal identification using morphometry of wheat grains. Biosyst. Eng. 94, 477–485.
Igathinathane, C., Prakash, V.S.S., Padma, U., Ravi Babu, G., Womac, A.R., 2006. Interactive computer software development for leaf area measurement. Comput. Electron. Agric. 51, 1–16.
Jeliński, T., Du, C.J., Sun, D.W., Fornal, J., 2007. Inspection of the distribution and amount of ingredients in pasteurized cheese by computer vision. J. Food Eng. 83, 3–9.
Li, Z., Hong, T.S., Wu, W.B., Liu, M.J., 2007. A novel method of object identification and leaf area calculation in multi-leaf image. ASABE Paper No: 073047. ASABE, St. Joseph, Michigan.
Maerz, N.H., 1998. Aggregate sizing and shape determination using digital image processing. In: Center For Aggregates Research (ICAR) Sixth Annual Symposium Proceedings, April 19–20, St. Louis, Missouri, pp. 195–203.
Momota, M., Miike, H., Hashimoto, H., 1994. Measuring particle size distribution by digital image processing with inverse Fourier–Bessel transformation. Jpn. J. Appl. Phys. 33, 1189–1194.
Mora, C.F., Kwan, A.K.H., Chan, H.C., 1998. Particle size distribution analysis of coarse aggregate using digital image processing. Cem. Concr. Res. 28, 921–932.
Rasband, W.S., 2007. ImageJ. U.S. National Institutes of Health, Bethesda, MD, USA, http://rsb.info.nih.gov/ij/index.html (Accessed February 2008).
Rodieck, B., 2007. EllipseFitter Class of ImageJ. http://rsb.info.nih.gov/ij/developer/source/ij/process/EllipseFitter.java.html (Accessed February 2008).
Sýkora, S., 2005. Approximations of Ellipse Perimeters and of the Complete Elliptic Integral E(x). A Review. http://www.ebyte.it/library/docs/math05a/EllipsePerimeterApprox05.html (Accessed February 2008).
Shahin, M., Symons, S.J.S., Poysa, V., 2006. Determining soya bean seed size uniformity with image analysis. Biosyst. Eng. 94, 191–198.
Yun, H.S., Lee, W.O., Chung, H., Lee, H.D., Son, J.R., Cho, K.H., Park, W.K., 2002. A computer vision system for rice kernel quality evaluation. ASABE Paper No. 023130. ASABE, St. Joseph, Michigan.